Enhanced Fluorescence Cell Imaging with Metal-Coated Slides

E. Le Moal,*† E. Fort,* S. Lévêque-Fort,† F. P. Cordelières,‡ M.-P. Fontaine-Aupart,† and C. Ricolleau*
*Laboratoire Matériaux et Phénomènes Quantiques (UMR 7162, Paris VII) and Laboratoire de Physique du Solide (UPR 5, ESPCI), F-75231 Paris cedex 05, France; †Laboratoire de Photophysique Moléculaire, CNRS UPR 3361, F-91405 Orsay cedex, France; and ‡Institut Curie Orsay, Plateforme d'Imagerie Cellulaire et Tissulaire, F-91405 Orsay cedex, France

ABSTRACT Fluorescence labeling is the prevailing imaging technique in cell biology research. When they involve statistical investigations on a large number of cells, experimental studies require both low magnification to get a reliable statistical population and high contrast to achieve accurate diagnosis on the nature of the cells' perturbation. Because microscope objectives of low magnification generally yield low collection efficiency, such studies are limited by the fluorescence signal weakness. To overcome this technological bottleneck, we proposed a new method based on metal-coated substrates that enhance the fluorescence process and improve collection efficiency in epifluorescence observation and that can be directly used with a common microscope setup. We developed a model based on the dipole approximation with the aim of simulating the optical behavior of a fluorophore on such a substrate and revealing the different mechanisms responsible for fluorescence enhancement. The presence of a reflective surface modifies both excitation and emission processes and additionally reshapes fluorescence emission lobes. From both theoretical and experimental results, we found the fluorescence signal emitted by a molecular cyanine 3 dye layer to be amplified by a factor ~30 when fluorophores are separated by a proper distance from the substrate. We then adapted our model to the case of homogeneously stained micrometer-sized objects and demonstrated mean signal amplification by a factor ~4. Finally, we applied our method to fluorescence imaging of dog kidney cells and verified experimentally the simulated results.

INTRODUCTION

Many biological studies and applications involve biomolecule detection by means of fluorescence. The use of fluorescent markers is notably the most widespread labeling technique for cell imaging. A large range of fluorophores with distinctive spectral characteristics are available, providing many possibilities for multi-color biological labeling. Moreover, most of the molecular fluorophores used in cell biology have been engineered to get a high biocompatibility. When associated with active biological molecules, molecular fluorophores allow specific labeling of cell entities (organelles, DNA, etc.) that play an essential role in cellular processes. Immunofluorescence technique is of particular interest because it allows detection of antigens involving their recognition by single dye-coupled antibodies. Using a multicolor set of functionalized dyes (biomarkers) and appropriate optical filters, one can thus selectively image parts of the cell or track several active biomolecules inside the cell.

Whereas biocompatibility and multi-color labeling are among the main advantages of these fluorescent molecules, their extinction coefficient is relatively weak compared with those of fluorescent nanoparticles (1). Consequently, the detection of low concentrations of fluorophores (even with quantum yield close to unity) is limited by the weakness of the fluorescence signal. When recorded intensity levels for subcellular structures become very close to the background, one can hardly draw cell contours or accurately distinguish where structures, such as microtubules, end. Generic image-processing algorithms have been reported (2), and deconvolution microscopies of particular interest have recently become widely used (3) but provide limited utility at low numerical aperture (NA).

Another drawback of molecular fluorophores is their low photostability. When excited, a fluorescent molecule may actually be involved in chemical reactions, especially with oxygen free radicals. This phenomenon, often referred to as photobleaching, causes the irreversible loss of the molecule fluorescence properties. Consequently, when an assembly of fluorophores is continuously excited, their emitted light progressively fades as light induces their destruction. Even though antifading may delay this destruction, this property is a strong drawback for dynamic studies, especially in time-lapse microscopy in which each frame is captured at a high rate (several tens of images per second). Signal intensities can then hardly be standardized. Reducing excitation power limits the photobleaching effects and thus delays the signal decay while obviously resulting in weaker fluorescence emission.

Signal weakness and photoreactivity have been partly overcome as a result of recent progress in the use of semiconductor nanocrystals, commonly called quantum dots, in biology (4). Quantum dots emit a more intense signal and have the advantage over molecular fluorophores that they do not suffer from photodestruction. However, they introduce new problems such as blinking of the emission signal and low biocompatibility that restrict the scope of in vivo applications. Despite the increasing interest raised by fluorescent nanoparticles, the

Submitted September 5, 2006, and accepted for publication November 17, 2006.

Address reprint requests to S. Lévêque-Fort, Laboratoire de Photophysique Moléculaire, CNRS UPR 3361, F-91405 Orsay cedex, France. E-mail: sandrine.fort@ppm.u-psud.fr.

0006-3495/07/03/2150/12 $2.00

doi: 10.1529/biophysj.106.096750

use of fluorescent molecules as markers for biomedical applications still has relevance and attractiveness.

In addition to the development of new fluorescent markers, the renewed interest in standard molecular fluorophores had been motivated by the development of innovative optical techniques for fluorescence enhancement. As a spontaneous emission process, fluorescence involves an interaction between the emitter and its environment and is therefore subject to external influence (5–7). It is thus possible to tailor the fluorescence process to increase emission intensity. The decay rate can be controlled by modifying the boundary conditions of the electromagnetic field. For instance, this can be made by setting the emitter close to a reflective (dielectric or metallic) surface. The interaction of a point emitter with a planar mirror has been described by a number of authors (5,8–19). Drexhage (5,9) used this configuration for the first time to verify experimentally the modification of the spontaneous emission rate. The author revealed this so-called mirror effect by measuring the variations in lifetime of excited Eu^+ ions as a function of their distance from a metal surface. In addition to emission changes, the presence of a mirror surface also modifies excitation rate and emission angular distribution, both of which argue in favor of detected signal amplification, provided that fluorophores are sited at a proper distance from it.

During the last 10 years, the use of fluorophore-metal interactions for fluorescence enhancement and its applications in biology have been widely investigated and reviewed (20–23). However, most of these works concerned either nonplanar systems, such as films of metal islands, or planar systems illuminated in configurations that require specific microscope devices. The latter works involved the excitation of plasmon modes at the metal surface. This process is known to yield intense optical fields at short distances from the metal surface (a few tens of nanometers, typically) and is thus not suitable when fluorescence enhancement is applied to micrometer-sized samples. To our knowledge, this is the first time that a theoretical and experimental study is reported on the enhancement of fluorescence for thick biological samples by means of a metal surface in epifluorescence observation.

Our approach is based on substrates developed from standard glass slides covered with metal and dielectric films (cf. diagram in Fig. 1). In this work, we consider fluorophores placed above a metallic surface and describe the physical mechanisms of fluorescence enhancement. To do so, the optical behavior of the fluorophores was simulated implementing a simple electric-dipole model and then compared with experimental observations. We then adapted the model to predict whether (and to what extent) our method still amplifies the detected fluorescence signal when applied to a micrometer-sized object such as a biological cell. A concrete example of application to cell imaging is presented, and mirror substrate interest and viability in a biomedical context are evaluated. As a conclusion of this work, potential improvements of the method are discussed.

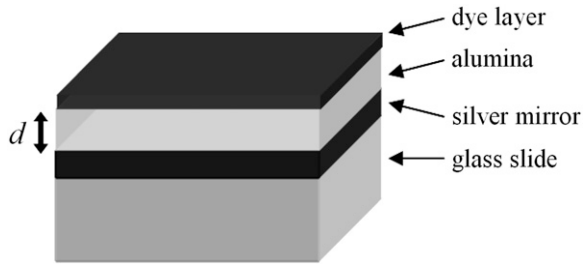

FIGURE 1 Active substrate coated with a dye layer; d stands for the thickness of the alumina layer separating fluorophores from the silver mirror surface.

METHODS

Substrate preparation

The substrates were prepared under ultrahigh-vacuum conditions on conventional coverslips or microscope slides. After standard cleaning procedures, a silver or gold deposition was performed by thermal evaporation. Metal films were thick enough (from 60 to 100 nm, typically) to limit light transmission in the visible spectrum so that metal-coated substrates behave like perfect mirrors. Before metal deposition, a thin layer of chromium was grown on the substrate surface to increase the metal film flatness and to ensure its adherence to the substrate. Morphology parameters of the metal layer were calculated from atomic force microscope images. Metal films were covered with a thin layer of amorphous alumina, obtained by pulsed laser deposition, to tune the sample-substrate distance and to endow the substrate surface with chemical properties similar to those of glass. Alumina layers, with thickness ranging from 1 nm to a few hundred nanometers, were achieved with a precision to the nanometer. An alumina layer of increasing thickness was obtained by partially hiding the slide surface with a mask and revealing it gradually throughout the deposition period. This way, many configurations were studied on the same sample, thus ensuring high reproducibility (24). Note that standard transmission imaging of the stained tissues remains possible on mirror slides exhibiting nonzero optical transmission. When metal layer thickness is 50 nm, reflectivity is sufficient to consider metal-coated slides as quasiperfect mirrors (reflection coefficient ranging from 89% to 98% for 452 nm $\leq \lambda \leq$ 632 nm), and light transmission is sufficient to image stained samples in transmission optical microscopy.

Dye layer deposition

To study fluorophore-substrate interaction, we coated substrate surface with thin films of dye fluorophores (cf. diagram in Fig. 1). Fluorophore interactions with the metal layer can be investigated precisely as a function of the spacing distance. This is, furthermore, a way to evaluate our method's efficiency for fluorophores presenting different quantum yields and spectral features. Indocarbocyanine (cyanine 3) has been chosen as model fluorophore in this study because these dye molecules are currently used as fluorescent labels for biological compounds. Cyanine 3 has a molar extinction coefficient of 150,000 $M^{-1}\,cm^{-1}$ at 552 nm, a quantum yield of ~0.15, and a maximum fluorescence emission at 570 nm (characteristics provided by Amersham Biosciences (Buckinghamshire, UK) with the Cy3 mono-reactive dye pack for protein labeling). Reagents, purchased from Amersham, were supplied in powder form and were diluted in absolute ethanol to obtain different concentrations. Dye thin films, ranging from one-thousandth to more than one monolayer in nominal thickness (i.e., molecular layers ranging from 10^{12} to 10^{15} molecules per 1 cm^2 in surface density), can be deposited by centrifugating a droplet of dye solution onto the substrate (spin-coating technique). However, a cleaner and more homogeneous method is thermal evaporation of solid dye under ultrahigh vacuum conditions after the deposition of metal and dielectric films. We used the latter technique for covering substrate surface with thin films of

fluorophores. Surface density was controlled a posteriori by transmission measurements performed with a conventional UV-visible-near infrared differential optical absorption spectrometer (Cary 5). Our study involved dye thin films with typical nominal thickness of one-tenth monolayer (surface density of 10^{14} molecules per 1 cm^2).

Immunofluorescence

The immunofluorescence technique commonly employs two sets of antibodies. A primary antibody is used against the antigen of interest and subsequently recognized by a secondary dye-coupled antibody. For this study, MDCK cells stably expressing eGFP-α-tubulin (generous gift from Dr. J. P. Dompierre) were grown as monolayers on the appropriate substrate for 48 h before fixation. Cells were lysed for 2 min in 0.5% Triton X-100 and fixed in 3% paraformaldehyde in PHEM buffer as described by Coquelle et al. (25). Cells were washed three times for 5 min in phosphate-buffered saline (PBS) and further permeabilized for 25 min in 0.1% Triton X-100 in PBS. Fixative was reduced by 50 mM NH_4Cl in PBS for 10 min, washed three times for 5 min in PBS, blocked in PBS/BSA 0.1% and labeled with a human polyclonal anti-GMAP-210 (26) and Mitotracker Red CMXRos (Molecular Probes, Carlsbad, CA) for 1 h at 37°C. After washing in PBS/BSA, the cells were incubated with secondary antibodies for 45 min (goat antihuman Alexa 633, Molecular Probes). The cells were postfixed in formaldehyde 4% in PBS for 16 min and treated by 50 mM NH_4Cl in PBS for 10 min. When indicated, the DNA was stained with DAPI (Sigma, St. Louis, MO) for 5 min. Coverslips were mounted using PBS/glycerol 1:1 containing 100 mg/ml of the antifading 1,4-diazabicyclo-(2.2.2)-octane (DABCO; Sigma). Excitation and fluorescence emission peak wavelengths are reported in Table 1 for each marker.

Three-dimensional wide-field optical sectioning fluorescence microscopy

Images of fixed cells were collected using a three-dimensional deconvolution imaging system described elsewhere (27,28). Briefly, the setup is made of a Leica DM RXA microscope, equipped with a 100× PlanAPO NA 1.4 oil immersion objective positioned by a PIFOC (piezoelectric translator, Physik Instrumente, Karlsruhe, Germany). Two air objective lenses (40× NA 0.55 and 20× NA 0.4) were additionally used with the aim of demonstrating the collection efficiency improvement on metal-coated substrates. A 5 MHz Micromax 1300Y interline CCD camera (Roper Instruments, Trenton, NJ) was used to collect stacks of fluorescence images 0.2 μm apart from each other in cases where the 100× objective was employed, the full system being under control of the Metamorph software (Molecular Devices, Wokingham, UK). A set of specific filter cubes was used to image each fluorescent marker channel (cf. Table 1).

Electric dipole model

We developed a model based on the dipole approximation with the aim of simulating the optical behavior of a fluorophore near plane surfaces of different natures. Results obtained with glass and silver surfaces were compared to reveal the different mechanisms responsible for fluorescence enhancement. Modeled systems are schematized in Fig. 2, *a* and *b*. Substrates were considered to be glass and metal slides of infinite thickness (semiinfinite space, one interface only). The latter assumption notably implies that the only losses of energy occurring when light is reflected at the metal surface are through absorption and not transmission through the metal film. A point dipole emitter was assumed to be in the air (ideal medium of refracted index equal to unity) and in close contact with the substrate surface. Distance from the metal was tuned by a layer of alumina, modeled as a nondispersive dielectric medium (refracted index equals 1.65) of finite thickness *d*. We neglected possible interactions with other emitters standing in the dipole neighborhood. We also assumed the emitter excitation and emission dipoles to be parallel.

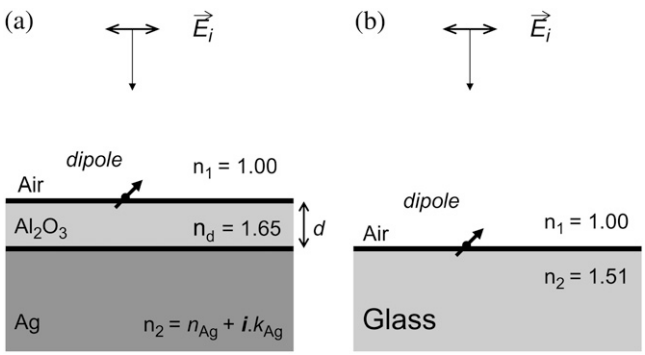

FIGURE 2 Geometry of the modeled systems. (*a*) Dipole at air/alumina interface above a semiinfinite silver substrate. (*b*) Dipole at the air/glass interface above a semiinfinite glass substrate. Plane wave illumination is achieved at normal incidence.

Molecule-substrate interaction was modeled using a purely classical description that was developed by Chance, Prock, and Silbey (CPS) (12,13). In CPS theory, the emitter is considered to be a forced damped dipole oscillator; damped because it radiates energy; forced because it responds to a part of its own field, which is reflected by the surface. The damping rate of the dipole depends on the phase relation between incident and reflective fields, which varies as a function of the distance from the surface (29). By using the complex dielectric permittivity of the metal, CPS theory describes the full optical response of the surface (reflection of the propagative field and energy transfer to the metal). For our study, we took complex dielectric permittivity of silver from Johnson and Christy (30). In CPS theory, the damping rate *b* of a forced damped dipole oscillator is given by Eq. 1 (*b* is normalized to its value b_0 in free space) where Q is the quantum yield of radiative decay (i.e., fluorescence quantum yield for a fluorophore); n_1 is the refractive index of medium 1 (cf. Fig. 2, *a* and *b*); μ_0 is the dipole momentum in free space; k_1 is the propagation constant of the electromagnetic wave emitted by the dipole in the medium 1 and is defined as the norm of the wave vector; E_0 is the complex amplitude of the reflected field at the dipole site, and $\mathrm{Im}(E_0)$ stands for its imaginary part:

$$b/b_0 = 1 + (3Qn_1^2)/(2\mu_0 k_1^3).\,\mathrm{Im}(E_0). \qquad (1)$$

The problem of the damping rate thus comes to the calculation of the reflected field at the dipole site. Dipoles with orthogonal and parallel orientations, with respect to the reflective interface, exhibit distinctive damping rates $b_\perp$ and $b_{//}$, respectively given by

TABLE 1 Characteristics of fluorophores and optical filters used for cell imaging

Fluorophore			Filter cube		
Name	Absorption	Fluorescence	Excitation	Dichroic	Emission
EGFP	489	508	BP 480/40	505	BP 527/30
Mitotracker Red CMXRos	579	599	BP 546/12	565	BP 600/40
Alexa 633	632	647	BP 620/60	660	BP 700/75

$$b_{\perp}/b_0 = 1 - (3/2)Q\,\mathrm{Im}\left\{\int_0^{\infty} r_{//}\exp(-2l_1 d')u^3/l_1\,\mathrm{d}u\right\} \quad (2)$$

$$b_{//}/b_0 = 1 - (3/4)\mathrm{Q}\,\mathrm{Im}\left\{\int_0^{\infty}[(1-u^2)r_{//} + r_{\perp}] \times \exp(-2l_1 d')u/l_1\,\mathrm{d}u\right\}, \quad (3)$$

where $r_{//}$ and $r_{\perp}$ stand for the reflection coefficients for incident rays polarized parallel (p-polarized) and orthogonal (s-polarized) to the plane of incidence, respectively; l_1 is defined by the relation $l_1 = -i(1 - u^2)$; d' equals $d\ k_1$ where d is the distance between the dipole and the reflective surface; u is the normalized in-plane component of the wave vector (6).

Equations 2 and 3 define total damping rates, i.e., integrated over all the emission components u of the dipole. However, all the emission components of the dipole are not modified similarly by the presence of the mirror surface. The reflected field intensity and phase at the dipole site indeed depend on the wave vector, i.e., the direction in which light is emitted. As a result, the presence of the mirror surface modifies the emission lobe shape. The angular distribution of the dipole emission can be retrieved from Eqs. 2 and 3. The emission components that belong to the range $u \in [0,1]$ correspond to radiative emission from the dipole, whereas those that belong to the complementary range $u \in]1,\infty[$ are associated with nonradiative emission, i.e., energy transfer (via dipole evanescent field) without emission of a photon. When considering the range $u \in [0,1]$, u equals the sine of the polar angle of emission θ, and the spatial radiation pattern of the dipole can be obtained from the integrand in Eqs. 2 and 3.

Another parameter that may be modified by the presence of a mirror surface is the excitation rate of the dipole. In the model presented here, excitation through a microscope objective was equated with a plane wave impinging the substrate surface at normal incidence. We thus did not consider the focusing of light onto the surface through an objective lens. The validity of such an approximation is limited to microscope objectives of low NA. Both the intensity and the phase of the reflected field had to be considered to calculate the excitation field at the dipole site. We applied Fresnel reflection laws at the interfaces of air/glass and air/alumina/silver systems (31). We will refer to the system of coordinates described in Fig. 3.

According to Malus' law, the efficiency of an incident electromagnetic wave to excite a dipole varies with the squared cosine of the angle formed by dipole momentum and electric field vectors. Dipole relative orientation with respect to the substrate surface plane (xy) is defined by the polar angle θ and the azimuthal angle φ. Assuming normal incidence, the excitation field only owns a component orthogonal to the incidence plane; hence, excitation efficiency equals $\cos^2(\pi/2 - \theta)$. We now consider an assembly of randomly oriented dipoles. The momentum of each dipole can be decomposed into a component parallel and a component orthogonal to the reflective interface.

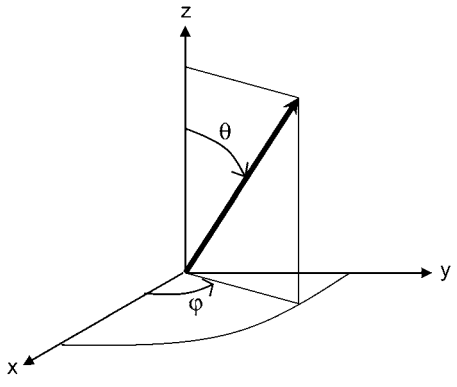

FIGURE 3 Coordinate system for describing dipole relative orientation with respect to the plane (xy) of the substrate surface; θ and φ are the polar and azimuthal angles, respectively.

The total power P, radiated by an assembly of N randomly oriented dipoles, can thus be given as a weighted sum of the powers emitted by parallel ($P_{//}$) and orthogonal ($P_{\perp}$) dipoles ideally excited (with efficiency equal to unity). Both excitation efficiency and emission components depend on dipole orientation, both have to be integrated over all possible dipole orientations. Hence, the expression of P is given by

$$P = (8/15)NP_{//} + (2/15)NP_{\perp}. \quad (4)$$

The complex problem of an assembly of randomly oriented dipoles thus comes to a much simpler problem. The former problem would have involved the simulation of a large number of dipoles, each exhibiting distinctive excitation and emission properties, depending on their orientation, whereas the latter is summed up in the simulation of a parallel and an orthogonal dipole, assuming both of them to be ideally excited.

RESULTS

The dipole model described above is implemented to simulate the optical behavior of an ideal emitter placed above a mirror substrate. To simplify understanding, fluorescence enhancement is decomposed into three main effects, related to fluorescence excitation, emission, and collection. The amplification factor gained from each effect is calculated for both orthogonal and parallel dipoles as a function of the distance from the metal. Note that the optical configuration considered here is epifluorescence observation, in which excitation and collection are achieved at the same side of the substrate and above the sample.

Excitation enhancement

Glass slides coated with smooth and continuous metal films act as perfect reflective surfaces. The interference between incoming and reflected electromagnetic fields leads to the formation of a standing wave close to the surface. Consequently, the excitation field intensity oscillates as a function of the distance from the mirror, alternating in-phase positions where the fluorophore excitation rate benefits from a fourfold enhancement and out-of-phase positions where the excitation rate decreases to zero. In other words, for proper separation distances, the apparent extinction coefficient of the fluorophore-substrate coupled system can be up to fourfold higher than the one of an isolated fluorophore.

In the context of this study, the proper reference to be considered for evaluating enhancement factors is a dipole in direct contact with a glass substrate rather than a dipole in free space. Our concern indeed is to evidence the improvement brought about by metal-coated substrates as compared with conventional bare glass slides. A dipole in direct contact with a glass surface actually experiences an excitation field, which intensity is lower than that of a dipole in free space because of the destructive interaction between incident and reflected fields. As a result, one may expect excitation enhancement factors to be higher than four for proper dipole-to-surface distances.

The excitation field was calculated at the dipole position for both configurations described above (separated from a mirror and in direct contact with glass), assuming a monochromatic illumination at 543 nm. The ratio between excitation field

intensities, termed relative excitation intensity, was plotted (cf. Fig. 4) as a function of the spacer layer thickness d. According to the model described above, normal incidence and plane wave illumination were assumed. The distance separating two maxima of intensity was found to equal half the wavelength in the dielectric medium ($\Delta d \approx 165$ nm for $\lambda_{exc} = 543$ nm and $n_d = 1.65$). An excitation enhancement by a factor ~6.2 was achieved for optimum distances (e.g., $d_1 = 58$ nm and $d_2 = 220$ nm). Because of the plane wave approximation, identical enhancement factors were found for larger optimum distances ($d_3 = 382$ nm, $d_4 = 543$ nm, $d_5 = 705$ nm, etc.). However, the actual strength of the excitation field intensity oscillations is expected to slightly decrease with increasing distance as a result of the true profile of the light beam.

Emission enhancement

Above a reflective surface, one can consider a fluorophore to be a dipole oscillator responding to its own field reflected from the mirror, i.e., a forced dipole oscillator. Depending on its delay, the reflected field will be in phase or out of phase, resulting in the decay rate being increased or reduced (29). The emission rate oscillates with increasing distance from the mirror, as the phase of the reflected field changes. When the emitted and reflected fields are in opposition of phase at the dipole site, a destructive interference is achieved, leading to the inhibition of the spontaneous emission process (32). After emission enhancement, the radiated power is amplified by a factor that is defined as the quantum yield relative variation. It is noteworthy that the worse initially the fluorophore (i.e., the lower the quantum yield in free space), the higher the emission enhancement factor. Conversely, although the emission rate may vary, no emission enhancement is expected from a fluorophore exhibiting a quantum yield equal to unity, whatever its position.

The actual improvement of fluorophore detection sensitivity is strongly related to the ratio between the number of photons detected (i.e., emitted toward the objective lens) and the number of photons absorbed by the fluorophores. This ratio depends on both emission and collection efficiencies and can be equated with an apparent quantum yield. We calculated this ratio for a dipole sited above a silver substrate, assuming collection through a NA 0.4 objective, and normalized it to that of a dipole directly adsorbed onto a glass substrate. Parallel and orthogonal dipoles were treated separately. Results were plotted as a function of the spacer layer thickness d (cf. Fig. 5). With the aim of simulating the optical behavior of cyanine 3 fluorophores, we assumed a monochromatic emission at $\lambda_{em} = 570$ nm and an initial quantum yield equal to $Q = 0.15$. Remarkably, the apparent quantum yields of parallel (*bold line*) and orthogonal (*thin line*) dipoles oscillate in opposition of phase because of the phase shift introduced by the field reflection on the substrate. However, this statement is not of major importance as long as dipole excitation efficiency is much larger for parallel than for orthogonal orientation, which is the case when a normal illumination is assumed.

One may notice that distances ensuring the greatest fluorescence enhancements approximately match those found for the highest excitation intensity. This is because of the very small difference between excitation and emission wavelengths and would not be true for fluorophores exhibiting a large Stokes shift, for instance. The gap between optimum distances for excitation and emission moreover increases proportionally to the distance from the substrate. Furthermore, peak coincidence is particularly apparent when illumination is achieved in normal incidence. The orthogonal component of dipole emission, which is poorly excited in normal incidence (cf. coefficients in Eq. 4), indeed exhibits maxima that do not match excitation maxima (cf. Fig. 5). Excitation in normal incidence is thus the most suitable configuration for fluorescence enhancement on a mirror substrate.

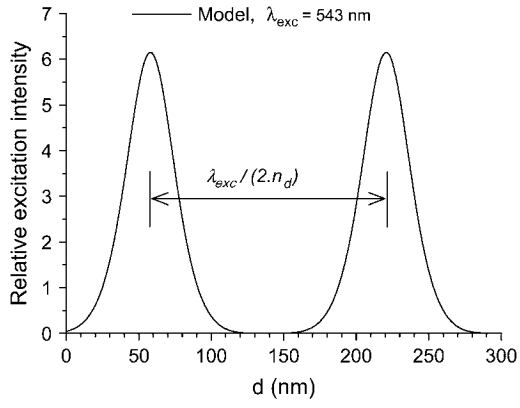

FIGURE 4 Excitation field intensity at the dipole site versus spacer layer thickness d, normalized to that of a dipole directly adsorbed onto a glass substrate. Excitation source is monochromatic, with $\lambda_{exc} = 543$ nm.

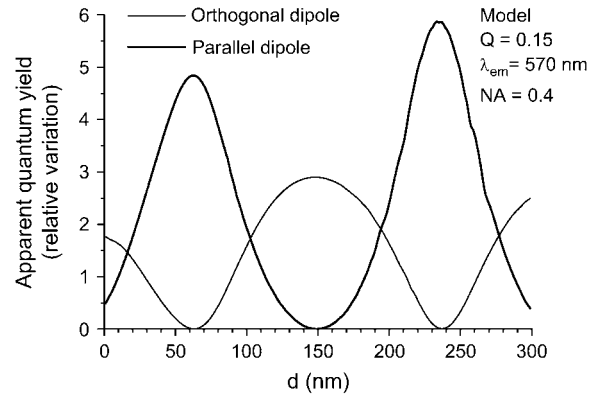

FIGURE 5 Apparent quantum yield of a dipole above a silver-mirror substrate versus spacer layer thickness d, normalized to that of a dipole directly adsorbed onto a glass substrate. Emitted light is assumed to be collected through a NA 0.4 objective. Thin and bold lines, respectively, stand for dipoles of orthogonal and parallel orientation with respect to the plane of the substrate surface.

Collection improvement

Besides the excitation enhancement, another contribution to the amplification of the detected signal is the redirection of the emitted light. Fig. 6 *a* is a diagram representing the angular distribution of the fluorescence emission (*spatial radiation pattern*), as calculated for an assembly of randomly oriented dipoles deposited on two different substrates. The radiated power was integrated over the azimuthal angle range and plotted as a function of the polar angle. A normal illumination at $\lambda_{exc} = 543$ nm was assumed, and dipole characteristics were those of cyanine 3 as given in the previous subsection. To consider random dipole orientation, we calculated the spatial radiation pattern for a parallel dipole and an orthogonal dipole; then we summed the two patterns weighted by the respective excitation efficiencies for dipolar emission components (cf. Eq. 4).

When the substrate is a common glass slide (*gray curve* in Fig. 6 *a*), fluorescence from adsorbed molecules is mostly emitted in the substrate because the refractive index is significantly higher in glass than in air. As a consequence, the collection efficiency is the lowest when excitation and collection are achieved at the same side of the substrate and above the sample, which is the case in numerous detection setups including, e.g., the epifluorescence microscope and commercial scanning devices for microarray readout. On the other hand, the vicinity of a metal surface modifies the spatial radiation pattern (*black curve* in Fig. 6 *a*). If the inert substrate is replaced by an optically active one, the emission lobe is redirected toward the objective lens, allowing the collection of up to ~80% of the emitted light, whereas only ~20% is collectable on standard substrates (24).

Because emission lobes show different shapes for the two different substrates, collection efficiency improvement depends on which part of the lobe is considered, i.e., the NA of the objective through which light is collected. In Fig. 6 *b*, fluorescence signal total enhancement, resulting from the three contributions described above (excitation, emission, and collection enhancement), was calculated for a given spacer layer thickness $d = 60$ nm and plotted as a function of collection objective NA. This enhancement factor corresponds to the ratio between black and gray curves in Fig. 6 *a*, integrated over a given polar angle range that was bounded by the maximum angle of collection. An enhancement by a factor of up to ~30 was achieved. Remarkably, signal enhancement decreases with increasing NA. Silver mirror substrates thus turn out to be of particular interest to amplify detected signal intensity with low-magnification (and low NA) objective lenses. However, the latter demonstration is restricted to the detection of fluorophores sited at well-defined distances from a substrate.

Comparison to experimental data

We investigated experimentally the fluorescence enhancement effect on model dye fluorophores, namely indocarbocyanine (cyanine 3), as a function of the distance from the mirror. To do so, we evaporated dyes on microscope slides that had been preliminary coated with a 60-nm-thick silver film. A spacer layer of alumina with increasing thickness was prepared as described above, in the subsection titled Sample Preparation. Optical observations were carried out on mirror substrates and bare glass slides to estimate the signal amplification. Fig. 7 depicts the enhancement factor as a function of the spacer layer thickness, as calculated from the model and as measured experimentally, and results are compared in Table 2. Experimentally, we observed a maximum enhancement by a factor ~26.7 for an optimum distance $d \sim 58$ nm (*first peak* in Fig. 7) and by a factor ~28.3 for $d \sim 225$ nm (*second peak*). Within the investigated range of distance (0–300 nm), we found a good agreement between model and experiment, with relative errors <10% for enhancement factor assessments. Moreover, theoretical calculations gave a very accurate estimation of the optimum distances (2% relative error). The full width at half-maximum (FWHM) was calculated for both experimental and theoretical enhancement peaks (cf. Table 2). As observed in Fig. 7, experimental peaks were found to be wider than theoretical ones (up to 25% relative error on the FWHM). However, this was expected because a monochromatic emission was assumed for modeling fluorophore behavior, whereas their actual fluorescence spectrum has a finite width.

Besides, when fluorophores are positioned on a mirror substrate at a separation distance *d* for which fluorescence is enhanced, the lifetime of their excited state is shortened (11). Remarkably, because the probability of photobleaching is proportional to the time a molecule spends in the excited

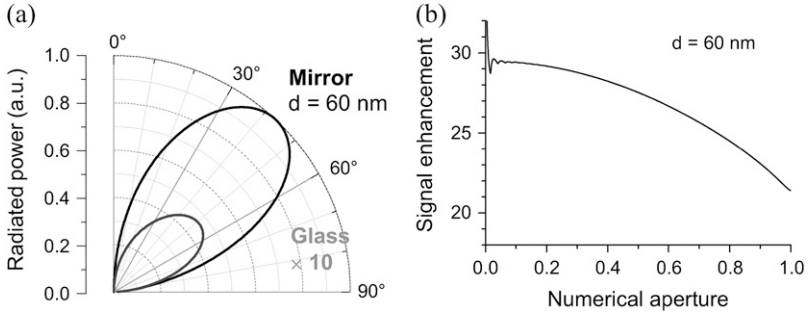

FIGURE 6 (*a*) Radiated power as a function of the polar angle (radiated power is integrated over the azimuthal angle [0 2π] range) calculated for an assembly of randomly orientated dipoles separated 60 nm from a silver surface (*black line*) and a similar assembly of dipoles directly adsorbed on a glass substrate (*gray line*). Please note that the latter data are multiplied by a factor 10 in the aim of making the comparison easier. (*b*) Fluorescence signal enhancement as a function of the NA of the objective through which light is collected.

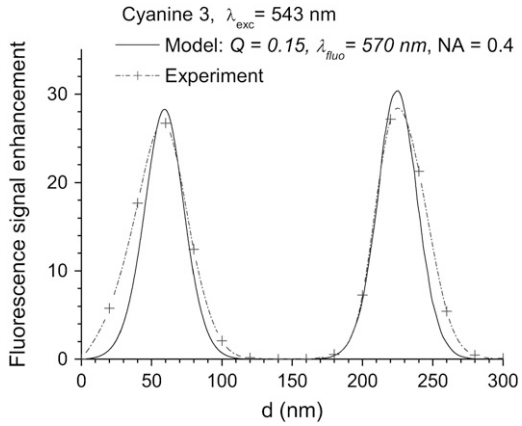

FIGURE 7 Fluorescence signal calculated for an assembly of randomly orientated dipoles separated a distance d from a silver surface. Collection is achieved through a NA 0.4 microscope objective. Fluorescence signal is normalized to that of a similar assembly of dipoles directly adsorbed onto a glass substrate. Theoretical calculations (*full black line*) are compared with experimental measurements (*gray crosses* and *dash-dot line*), which were obtained from a 0.1 monolayer film of cyanine 3 dye fluorophores evaporated onto an active substrate.

state, lifetime shortening results in fluorophore photostabilization (33). For $d = 60$ nm, we experimentally found lifetimes to be ~2-fold shorter (24) and the number of emitted photons before fluorophore photodestruction to be ~2-fold larger, as compared with fluorophores adsorbed on a standard glass slide.

One of the most prominent features of fluorescence at metal surfaces is the strong canceling of fluorescence emission in the first 10 nm of the surface. This phenomenon, commonly termed fluorescence quenching, results from fast energy transfer to the substrate by near-field coupling of the dipole field (33). This effect is implicit in the CPS classical dipole theory used here (12). As can be seen in Fig. 7, fluorescence detection from a fluorophore within the first 10 nm of a metal surface is much worse than that on bare glass. Note that charge transfer additionally contributes to fluorescence quenching when a fluorophore is directly adsorbed onto a metal surface (34). However, the optimum fluorophore-metal distances for excitation and emission enhancement are always larger than 10 nm when the observation configuration is epifluorescence. Therefore, fluorescence quenching does not significantly reduce the efficiency of the method presented here.

Until now, we modeled the optical behavior of a molecular layer that was considered to be infinitely thin. All the fluorophores of the molecular layer were assumed to be separated from the substrate by a constant distance. From here, we examine samples of finite thickness.

TABLE 2 Results from the analysis of Fig. 7

	1st peak			2nd peak		
	Experiment	Model	Relative error	Experiment	Model	Relative error
Distance (nm)	58	59	0.02	225	225	< 0.01
Enhancement	26.7	28.4	0.06	28.3	30.5	0.08
FWHM (nm)	43.6	32.9	0.25	39.4	33.0	0.16

Fluorescence enhancement for micrometer-sized objects

Excitation and emission enhancement effects are particularly attractive for studies on biological processes occurring close to the surface or at a well-defined distance from it (e.g., binding of a target analyte to a receptor on the surface of a biosensor; hybridization of DNA to the oligonucleotide probes in a microarray (35)). However, the distribution of fluorophore-mirror distances is much wider when the labeled object is a micrometer-sized biological cell. The excitation enhancement is thus averaged over the cell thickness, resulting in a lower amplification. Nevertheless, the mean excitation rate is expected to be about twice as high on a mirror compared with a glass slide. Indeed, if we assume the substrate to be perfectly reflective and we disregard the attenuation of light after propagation into the sample, then we can consider that the mean intensity of the excitation field, inside the sample, is twofold higher than if the substrate were perfectly transparent.

Previously we saw that fluorophore emission rate oscillates as its separation from the mirror changes. However, the strength of these oscillations decreases as the distance from the reflective surface increases, because of the emitter point source nature. Consequently, emission enhancement plays an important part for very thin samples only. Detected signal amplification for thick samples is thus mainly caused by the increase of fluorophore excitation rate and fluorescence collection efficiency. Similarly, substrate influence on fluorophore photostability is expected to be very small once it is averaged over several micrometers.

When the distance from the mirror is much longer than excitation wavelength, one has furthermore to grant importance to the slight spectral gap between fluorescence excitation and emission. Several microns away from the surface, excitation and emission field might significantly be out of phase, resulting in low fluorescence efficiency.

Now the main question is whether (and to what extent) the use of mirror substrates still helps fluorophore detection when applied to micrometer-scaled objects such as biological samples. To solve this issue, we adapted our model to a new system, which is depicted in Fig. 8. We considered a biological sample directly adsorbed on the substrate surface, immersed in an aqueous medium, and homogeneously stained with fluorophores. Sample and its medium refractive indices were assumed to equal that of water ($n = 1.33$). Again, substrates were equated with semiinfinite spaces. Only one interface was considered, namely a glass/water or metal/water interface. All the d-dependant functions calculated before (excitation rate, radiative yield, radiation spatial pattern, etc.) were integrated over a given range of distance,

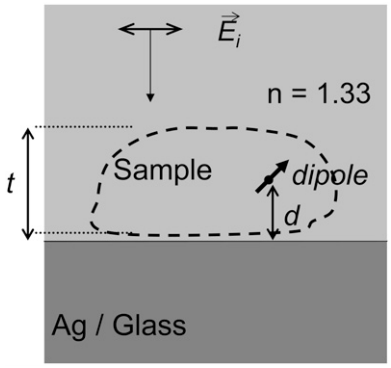

FIGURE 8 Geometry of the modeled system; homogeneous sample is considered to be adsorbed at substrate surface; sample and sample medium refractive indices are assumed to equal that of water ($n = 1.33$); t stands for sample thickness.

corresponding to the thickness, t, of the sample, assuming a uniform distribution of fluorophore-to-substrate distances.

Fig. 9 presents the mean amplification of the signal intensity, calculated as a function of the sample thickness t. Two different NAs were considered, namely NA = 0.4 (*black line*) and NA = 0.55 (*gray line*). A mean amplification of the signal intensity by a factor ~3.9 was obtained for a 5-μm-thick sample, assuming monochromatic excitation at $\lambda_{exc} = 489$ nm and fluorophore characteristics similar to that of eGFP ($Q = 0.6$, $\lambda_{em} = 508$ nm). For values that equal ~4 wavelengths in the sample medium typically ($t \sim 1.5$ μm for $n_d = 1.65$), the mean intensity enhancement of the fluorescence signal does not vary much with increasing sample thickness. A relative variation of ±5% was observed for thicknesses ranging from 1.5 to 5 μm. When the sample thickness is varied, the angular distribution of fluorescence emission evolves, thus modifying collection efficiency. This variation gets weaker when light is collected through an

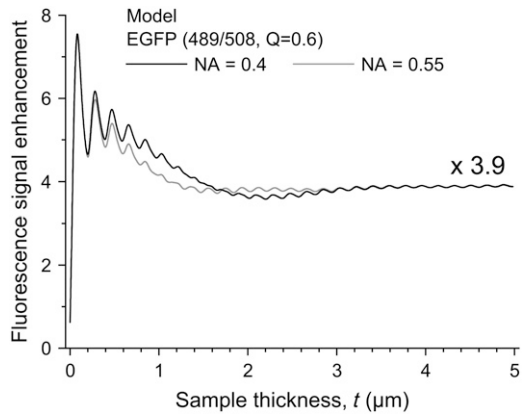

FIGURE 9 Fluorescence signal enhancement, calculated by averaging fluorescence enhancement factor over the sample thickness. Fluorophore distribution into the sample is assumed to be homogeneous. Fluorophore characteristics are similar to that of eGFP. Light collection is achieved through NA 0.4 (*black line*) and NA 0.55 (*gray line*) objective lenses. A mean amplification by a factor 3.9 is obtained for a 5-μm-thick sample.

objective lens of higher NA (±3% relative variation for NA = 0.55). One can thus expect a relative constancy of the signal amplification factor when the sample thickness varies from one region to another, which is the case in cell-imaging applications. Moreover, the model yielded similar results when the characteristics of eGFP were replaced by those of Mitotracker Red CMXRos ($\lambda_{exc} = 579$ nm, $\lambda_{em} = 599$ nm) and Alexa 633 ($\lambda_{exc} = 632$ nm, $\lambda_{em} = 647$ nm), notably mean amplifications of the signal intensity by a factor ~3.9 (Mitotracker) and a factor ~3.8 (Alexa 633).

Another important point for cell-imaging applications is the method efficiency with low-magnification objective lenses. When considering dye thin films, we demonstrated particular interest in silver mirror substrates for detected signal amplification with microscope objectives of low NA. Similar investigations were carried out on fluorescence enhancement for thick samples. Fig. 10 *a* is a diagram representing the spatial radiation pattern, as calculated for a 5-μm-thick homogeneously stained sample and for two different substrates, namely a silver mirror (*black line*) and a glass surface (*gray line*). Diagrams presented in Figs. 6 *a* and 10 *a* were built up similarly. A normal illumination at $\lambda_{exc} = 489$ nm is assumed, and fluorophore characteristics are those of eGFP as given in the previous subsection. First of all, emission lobes presented in Figs. 6 *a* and 10 *a* exhibit very distinctive aspects. Notably, the emission distribution is significantly larger at wide angles when a thick sample is used. The collection efficiency is thus limited when light is collected through an objective lens of low NA. However, the use of a reflective surface amplifies the intensity of the detected signal even when a low-NA objective is used, as illustrated by Fig. 10 *b*. Enhancement of fluorescence signal intensity, which corresponds to the ratio between black and gray curves in Fig. 10 *a*, was plotted as a function of collection objective NA. Contrary to the case presented in Fig. 6 *b*, signal enhancement remains relatively constant with increasing NA (relative variation of ±1% for NA ranging from 0.3 to 1.0). Finally, the use of a silver mirror substrate, instead of a bare glass slide, is expected to amplify the intensity of the detected signal by at least a factor 3.9, even when light is collected through a low-NA objective lens.

Application to cell imaging

We applied our method to fluorescence imaging of dog kidney cells, which are model subjects for the study of subcellular structures within epithelial cells, especially in the context of cancer research (36). Statistical studies carried out on epithelium cells allow evaluating the proportion of cells that exhibit an abnormal inner structure. Such studies require both wide field (low magnification) to get a reliable statistical population and high contrast (high signal and signal/noise ratio) to achieve an accurate diagnosis. Experimental works were carried out to demonstrate the interest of active substrates for the enhancement of fluorescence image brightness and contrast.

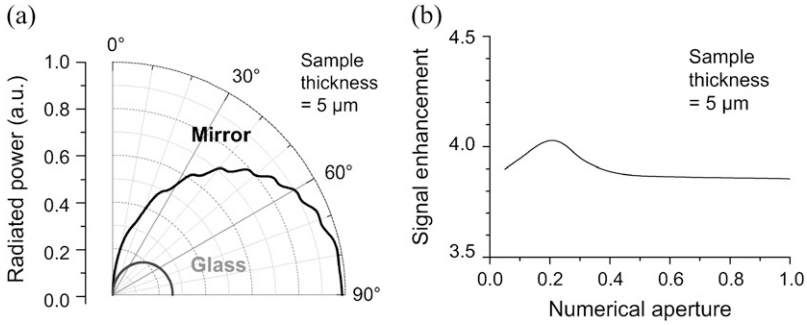

FIGURE 10 (*a*) Radiated power as a function of the polar angle (radiated power is integrated over the azimuthal angle [0 2π] range) calculated for a 5-μm-thick homogeneously stained sample adsorbed onto a silver (*black line*) or glass (*gray line*) substrate. (*b*) Fluorescence signal enhancement as a function of the NA of the objective through which light is collected.

We grew a monolayer of dog kidney cells onto a mirror substrate, namely a microscope slide previously coated with a 60-nm-thick silver layer. Cells were fluorescently labeled following the immunofluorescence technique described above. Cell microtubules were tagged with eGFP, Golgi network with Alexa 633, and mitochondria with Mitotracker Red CMXRos. Fig. 11 *a* is an overlay of three fluorescence images obtained with three different sets of filters (cf. Table 1), each image corresponding to the detection of one of the three biomarkers used for labeling the cells (*green* for Alexa 633, *blue* for Mitotracker, and *red* for eGFP). Fluorescence signal was collected through a 20× NA 0.4 air objective, in epifluorescence configuration. In Fig. 11 *a*, the silver film was scratched so that a stripe is deprived of metal and lets the bare glass slide reveal itself below (*dark region* in the *left part* of *image*). The signal collected from cells sited in the latter stripe served as reference for evaluating the signal enhancement factor. Another region of the substrate (*dark*

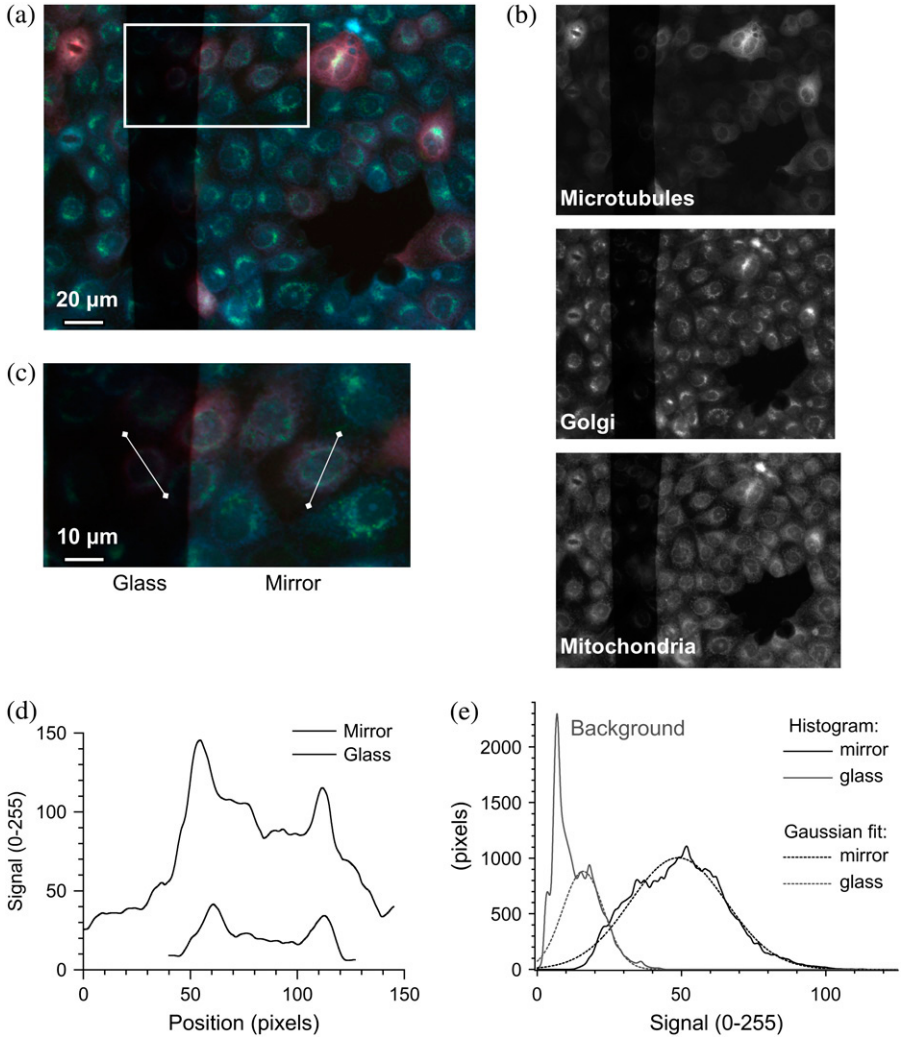

FIGURE 11 (*a*) Dog kidney cells adsorbed onto an active substrate, fluorescence image in false colors. Red, green, and blue colors are respectively associated with cell microtubules, Golgi networks, and mitochondria. Fluorescence signal is detected through a 20× NA 0.4 microscope objective. A region of the substrate is deprived of silver (*dark vertical stripe* at the *image left side*) so that the sample is in direct contact with the bare glass surface. Measurements from this region are used as reference for enhancement factor calculation. (*b*) Fluorescence images corresponding to each signal channel (*red, green, blue*) of *a*. (*c*) Magnification of a region of interest taken from *a* (*white frame*) exhibiting both coated (*right side*) and uncoated (*left side*) areas. (*d*) Profile plots across cells from the uncoated (*gray line*) and coated (*black line*) areas of *c*. (*e*) Signal histograms calculated for coated (*mirror*) and uncoated (*glass*) regions of *a* fluorescence image, considering the signal detected from mitochondrial probes (Mitotracker Red CMXRos) only.

and *uniform area* at *bottom right corner* of Fig. 11 *a*) is without cells, allowing one to measure the signal background on the metal-coated surface directly. In Fig. 11 *b*, signal channels (*red, green, blue*) of the color image in Fig. 11 *a* are split to show microtubule, Golgi network, and mitochodrion staining separately. Fig. 11 *c* is a magnification of a region of interest taken from Fig. 11 *a* that comprises an uncoated area (*left side*) and a metal-coated area (*right side*). Signal intensity profile was calculated for a cell from each area to demonstrate the signal amplification. Gray and black lines in Fig. 11 *d* represent the signal measured along white segments in Fig. 11 *c*. From Fig. 11 *d*, we roughly estimated the signal intensity to be amplified by a factor between 3 and 4.

To demonstrate the improvement brought about by the use of mirror substrates in fluorescence detection (and accurately measure signal amplification factor), we statistically studied the signal variations over wide areas of the substrate, comprising more than 100 cells. The pixel intensity distribution was investigated on both metal-coated and uncoated regions using the ''histogram'' function of ImageJ (W. S. Rasband, ImageJ, U. S. National Institutes of Health, Bethesda, MD, http://rsb.info.nih.gov/ij/, 1997–2006). With the assumption that the cells were evenly distributed on the substrate, the mean fluorescence intensity and its standard deviation were recovered from signal histograms by fitting experimental data with Gaussian profiles. The histogram shown in Fig. 11 *e* was built considering specifically fluorescence emission from mitochondrial probes (Mitotracker Red CMXRos); results from histogram analysis are gathered in Table 3. The mean background levels were measured in regions without cells and used as a basis for evaluating signal/noise ratios on both metal-coated and uncoated regions. As reported in Table 3, we found the mean intensity of the fluorescence signal to be amplified by a factor 3.1, which is in good agreement (~20% relative error) with what we calculated with our model (3.9 for Mitotracker Red CMXRos, assuming NA = 0.4). Not only was the signal intensity increased but also the signal/noise ratio, by a factor 1.5, thus yielding better fluorescence contrast. For both metal-coated and uncoated regions, we characterized the width of the signal intensity distribution by calculating its relative standard deviation, *i.e.*, the half-width at half-maximum of the Gaussian profile normalized by its maximum intensity. Quite similar values were found, pleading for homogeneous enhancement of fluorescence emission, the signal being amplified independently of its intensity. Fluorescence images corresponding to Alexa-633 labeling were similarly treated, and we found a mean signal amplification by a factor 4.5, which again is quite close to the model results (<15% relative error).

Quantifications were also done on fluorescence images obtained using a 40× NA 0.55 air objective and a 100× NA 1.4 oil immersion objective. Surprisingly, although enhancement efficiency was confirmed by measurements done with NA 0.55 objective, relatively poor results were obtained when light was collected with the highest NA objective. Signal intensity collected with the NA 1.4 oil immersion objective was found to be amplified by a factor ~1.6. Moreover, the use of a mirror surface with a high-NA objective turned out to cause a relative loss of contrast. Although the background remained very low on metal-coated regions without biological material, cell contour appeared with less sharpness above the mirror substrate. Several reasons may explain this phenomenon, the main one being related to the image lateral resolution. In Fig. 12, an objective lens collects the emitted light from a point source positioned in its focus plane and at a distance *d* from a mirror surface. The part of the emitted light that is reflected by the mirror before being collected contributes to raising the signal level only if it cannot be separated from the direct light in the image formed by the objective. On the contrary, if reflected light collected through the objective forms a spot in the focus plane that is larger than the image resolution, then a significant part of it will only contribute to alter the image contrast and apparent resolution.

TABLE 3 Results from the analysis of Fig. 11e

	Background	Mean signal	Mean SNR*	Rel. SD†
Glass	6.9	15.9	2.3	0.22
Mirror	14.4	48.9	3.4	0.17
Enhancement	2.1	3.1	1.5	0.8

*Signal/noise ratio.
†Relative standard deviation.

DISCUSSION

Limits of the model

In considering a homogeneously stained object similar in size to a cell, all the effects brought about by the presence of

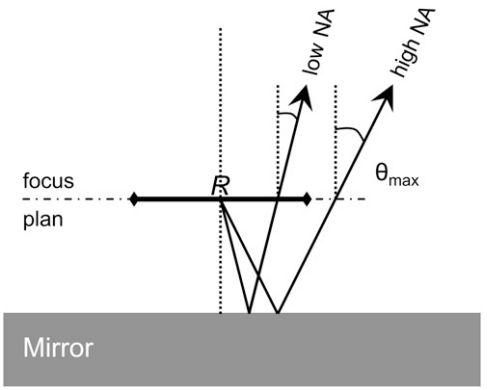

FIGURE 12 Geometric representation of a point emitter *E* placed above a mirror surface and in the focus plane of an objective lens (*horizontal dash-dot line*). The lateral resolution achieved with the objective is schematized by a horizontal bold segment in the focus plane. Arrows originating from *E* represent light emission at the maximum angles of collection of the objective lens for two different NA. For low NA, all the light collected after being reflected by the mirror is associated with the point emitter *E* in the image formed by the objective lens.

a reflective surface are averaged over its thickness and thus may yield lower enhancement than for a single fluorophore. In particular, we found the effect on fluorophore emission rate to be negligible once averaged over the whole assembly of fluorophores spread over the volume of the micrometer-sized object. Consequently, the mean enhancement factor is not expected to differ significantly for fluorophores of different quantum yields. Similarly, when the object thickness is large compared with the excitation and emission wavelengths, the mean enhancement factor is not expected to depend on fluorophore spectral features (excitation and emission spectra). However, we investigated fluorescence enhancement for the three different biomarkers used for labeling cells in this study (cf. Table 1), and we found slight differences. Fluorescence from Mitotracker Red CMXRos and Alexa 633 biomarkers (which were used for labeling mitochondria and Golgi networks, respectively) showed good agreement with the model, whereas lower enhancement factors ($\sim$2.5 with NA 0.4 air objective, $\sim$2.1 with NA 0.55 air objective, $\sim$1.8 with NA 1.4 oil objective) were found for eGFP biomarkers, which were used for labeling cell microtubules. Several reasons may explain this difference. On one hand, eGFP exhibits high quantum yield ($Q \approx 0.6$) and may thus benefit from lower emission enhancement than other fluorophores. However, when a thick sample is considered, the mean enhancement factor does not significantly depend on fluorophore quantum yield (the latter statement is demonstrated above in the subsection ''Fluorescence enhancement for micrometer-sized objects''). On the other hand, fluorophores are not homogeneously distributed over the sample bulk as assumed in the model. Biomarkers are localized at the site of the labeled organelles in the cell, which organelles may be more or less close to the substrate surface, hence benefiting more or less efficiently from its effect. A more realistic simulation would consider a typical heterogeneous distribution of fluorophores, depending on the labeled organelle's position in the cell.

Potential improvements of the method

Substrate surface chemical reactivity is of major importance, notably for growing cells. In most biological applications, gold may be preferred as coating metal because of its high biocompatibility. Moreover, coating substrates with gold rather than silver prevents metal oxidation drawbacks. Indeed, the thin layer of silver oxide that may form at the metal surface modifies its optical properties. Once photoactivated, silver oxide is known to become photoluminescent, with wide excitation and emission spectra (37,38). This phenomenon yields additional noise that can hardly be filtered and, although weak, alters the signal/noise ratio. Substrate surface may also be protected by coating it with a thin layer of a transparent and isolating material acting as a barrier to oxidation. However, the isolating material chemical reactivity needs to suit cell growth.

The principle of fluorescence enhancement on metal-coated substrates is based on their ability to reflect the light illuminating the sample and the light emitted by fluorophores. Their efficiency thus requires the metal film to act as a perfect mirror at excitation and emission wavelengths. Typically, the reflection coefficients at silver/water and gold/water interfaces drop for wavelengths shorter than 340 nm and 580 nm, respectively. As an example, a very shallow fluorescence enhancement is expected from a sample stained with DAPI ($\lambda_{exc} = 365$ nm, $\lambda_{fluo} = 420$ nm) and sited above a gold substrate. Other metals, such as aluminum and platinum, should be considered for extending substrate reflectivity toward the near-UV range.

Outlooks on the application of metal-coated substrates in cell biology

In cell biology, all scales count: one may have a view of the global architecture of a tissue while wanting to have access to higher, more subtle details. Although low magnification allows the former, the biologist might be limited by the low light collected using low magnification and a small-NA objective. Even using amplification systems as in indirect immunofluorescence on fixed samples, it may be hard to extract valuable information from weakly stained samples. All technologies aiming to increase signals are therefore of major interest. Use of metal coating may be one of those.

Another field of application for this technique may be live cell imaging. Over the past decade videomicroscopy has become a widespread means to follow dynamic events within the entire volume of a cell. Although the protein engineering has allowed significant progress to be done in the field of genetically encoded fluorescent markers, the problem remains of live samples being sensitive to light irradiation. One particular example is the susceptibility of cells to UV irradiation, especially as they enter mitosis (39). The current compromise is to lower the intensity of excitation source while inducing a loss in the emitted light detected. The use of metal-coated substrates in such a situation in the future could be a good alternative both to redirect excitation that crosses the sample and to help collection of emitted light while keeping the same irradiation level.

The authors thank Romain Briandet (INRA, Massy, France) for valuable discussions and help with some of the experiments. The authors also thank Ariane Deniset.

This work was supported by the French Research Ministry and the National Center for Scientific Research (CNRS) through the Nanoscience-Nanotechnology Program and the DNA Biochip Program.

REFERENCES

1. Seydack, M. 2005. Nanoparticle labels in immunosensing using optical detection methods. *Biosens. Bioelectron.* 20:2454–2469.

2. Altinok, A., B. Sumengen, B. S. Manjunath, and K. Rose. 2006. Reducing incidental fluorescence in live cell imaging. *In* Technical Report. ECE, UCSB.

3. Sibarita, J.-B. 2005. Deconvolution microscopy. *In* Microscopy Techniques. Rietdorf J, editor. *Advances in Biochemical Engineering/Biotechnology*. Springer Verlag, Heidelberg. 201–243.

4. Dubertret, B., P. Skourides, D. J. Norris, V. Noireaux, A. H. Brivanlou, and A. Libchaber. 2002. In Vivo Imaging of Quantum Dots Encapsulated in Phospholipid Micelles. *Science*. 298:1759–1762.

5. Drexhage, K. H. 1974. *In* Progress in Optics, Vol. XII. Wolf E, editor. North-Holland, Amsterdam 163–232.

6. Barnes, W. L. 1998. Fluorescence near interfaces: the role of photonic mode density. *J. Mod. Opt.* 45:661–699.

7. Lakowicz, J. R. 1999. Introduction to fluorescence. *In* Principles of fluorescence spectroscopy. Academic K, editor. 2nd ed. Plenum Press, New York. 1–21.

8. Morawitz, H. 1969. Self-coupling of a two-level system by a mirror. *Phys. Rev.* 187:1792–1796.

9. Drexhage, K. H. 1970. Influence of a dielectric interface on fluorescence decay time. *J. Luminescence.* 1–2:693–701.

10. Tews, K. H. 1974. On the variation of luminescence lifetimes. The approximations of the approximative methods. *J. Luminescence.* 9: 223–239.

11. Chance, R. R., A. Prock, and R. Silbey. 1974. Lifetime of an emitting molecule near a partially reflecting surface. *J. Chem. Phys.* 60:2744–2748.

12. Chance, R. R., A. Prock, and R. Silbey. 1975. Comments on the classical theory of energy transfer. *J. Chem. Phys.* 62:2245–2253.

13. Chance, R. R., A. Prock, and R. Silbey. 1976. Comments on the classical theory of energy transfer. II. Extension to higher multipoles and anisotropic media. *J. Chem. Phys.* 65:2527–2531.

14. Burghardt, T. P., and N. L. Thompson. 1984. Effect of planar dielectric interfaces on fluorescence emission and detection. Evanescent excitation with high-aperture collection. *Biophys. J.* 46:729–737.

15. Hellen, E. H., and D. Axelrod. 1987. Fluorescence emission at dielectric and metal-film interfaces. *J. Opt. Soc. Am. B.* 4:337–350.

16. Ford, G. W., and W. H. Weber. 1984. Electromagnetic interactions of molecules with metal surfaces. *Phys. Rep.* 113:195–287.

17. Pockrand, I., A. Brillante, and D. Mobius. 1980. Nonradiative decay of excited molecules near a metal surface. *Chem. Phys. Lett.* 69:499–504.

18. Lukosz, W., and R. E. Kunz. 1977. Light emission by magnetic and electric dipoles close to a plane interface. I. Total radiated power. *J. Opt. Soc. Am.* 67:1607–1615.

19. Lukosz, W., and R. E. Kunz. 1977. Light emission by magnetic and electric dipoles close to a plane dielectric interface. II. Radiation patterns of perpendicular oriented dipoles. *J. Opt. Soc. Am.* 67:1615–1619.

20. Lakowicz, J. R. 2001. Radiative decay engineering: biophysical and biomedical applications. *Anal. Biochem.* 298:1–24.

21. Lakowicz, J. R., Y. Shen, S. D'Auria, J. Malicka, J. Fang, Z. Gryczynski, and I. Gryczynski. 2002. Radiative decay engineering: 2. Effects of silver island films on fluorescence intensity, lifetimes, and resonance energy transfer. *Anal. Biochem.* 301:261–277.

22. Lakowicz, J. R. 2005. Radiative decay engineering 5: metal-enhanced fluorescence and plasmon emission. *Anal. Biochem.* 337:171–194.

23. Aslan, K., I. Gryczynski, J. Malicka, E. Matveeva, J. R. Lakowicz, and C. D. Geddes. 2005. Metal-enhanced fluorescence: an emerging tool in biotechnology. *Curr. Opin. Biotechnol.* 16:55–62.

24. Le Moal, E., S. Lévêque-Fort, E. Fort, J.-P. Lacharme, M.-P. Fontaine-Aupart, and C. Ricolleau. 2005. Active substrates improving sensitivity in biomedical fluorescence microscopy. *Proc. SPIE Int. Soc. Opt. Eng.* 5860:58600G.

25. Coquelle, F. M., M. Caspi, F. P. Cordelieres, J. P. Dompierre, D. L. Dujardin, C. Koifman, P. Martin, C. C. Hoogenraad, A. Akhmanova, N. Galjart, J. R. De Mey, and O. Reiner. 2002. LIS1, CLIP-170's key to the dynein/dynactin pathway. *Mol. Cell. Biol.* 22:3089–3102.

26. Infante, C., F. Ramos-Morales, C. Fedriani, M. Bornens, and R. M. Rios. 1999. GMAP-210, a *cis*-Golgi network-associated protein, is a minus end microtubule-binding protein. *J. Cell Biol.* 145:83–98.

27. Savino, T. M., J. Gebrane-Younes, J. De Mey, J.-B. Sibarita, and D. Hernandez-Verdun. 2001. Nucleolar assembly of the rRNA processing machinery in living cells. *J. Cell Biol.* 153:1097–1110.

28. Sibarita, J.-B., H. Magnin, and J. De Mey. 2002. Ultra-fast 4D microscopy and high throughput distributed deconvolution. *Proc. IEEE Int. Symp. Biomed. Imaging*. 769–772.

29. Amos, R. M., and W. L. Barnes. 1997. Modification of the spontaneous emission rate of Eu^{3+} ions close to a thin metal mirror. *Phys. Rev. B.* 55:7249–7254.

30. Johnson, P. B., and R. W. Christy. 1972. Optical constants of the noble metals. *Phys. Rev. B.* 6:4370–4379.

31. Arnoldus, H. F. 2004. Power emitted by a multipole near an interface. *Surf. Sci.* 571:173–186.

32. Yablonovitch, E. 1987. Inhibited spontaneous emission in solid-state physics and electronics. *Phys. Rev. Lett.* 58:2059–2062.

33. Enderlein, J. 1999. Single-molecule fluorescence near a metal layer. *Chem. Phys.* 247:1–9.

34. Gebauer, W., A. Langner, M. Schneider, M. Sokolowski, and E. Umbach. 2004. Luminescence quenching of ordered π-conjugated molecules near a metal surface: Quaterthiophene and PTCDA on Ag(111). *Phys. Rev. B.* 69:155431–155438.

35. Choumane, H., N. Ha, C. Nelep, A. Chardon, G. O. Reymond, C. Goutel, G. Cerovic, F. Vallet, C. Weisbuch, and H. Benisty. 2005. Double interference fluorescence enhancement from reflective slides: Application to bicolor microarrays. *Appl. Phys. Lett.* 87:031102.

36. Vasiliev, J. M., T. Omelchenko, I. M. Gelfand, H. H. Feder, and E. M. Bonder. 2004. From the Cover: Rho overexpression leads to mitosis-associated detachment of cells from epithelial sheets: A link to the mechanism of cancer dissemination. *Proc. Natl. Acad. Sci. USA.* 101: 12526–12530.

37. Peyser, L. A., A. E. Vinson, A. P. Bartko, and R. M. Dickson. 2001. Photoactivated fluorescence from individual silver nanoclusters. *Science.* 291:103–106.

38. Boyd, G. T., Z. H. Yu, and Y. R. Shen. 1986. Photoinduced luminescence from the noble metals and its enhancement on roughened surfaces. *Phys. Rev. B.* 33:7923–7936.

39. Rieder, C. L., and R. W. Cole. 1998. Entry into mitosis in vertebrate somatic cells is guarded by a chromosome damage checkpoint that reverses the cell cycle when triggered during early but not late prophase. *J. Cell Biol.* 142:1013–1022.